Noname manuscript No.
(will be inserted by the editor)

A Parametric Intensity-Based 3D Image Registration Method for Magnetic Resonance Imaging

Huajun Song · Peihua Qiu

Received: date / Accepted: date

Abstract Image registration (IR) aims to map one image to another of a same scene. With rapid progress in image acquisition technologies, 3D IR becomes an important problem in magnetic resonance imaging (MRI) and other applications. In the literature, however, most IR methods are for 2D images and there are only a limited number of 3D methods available. Because 3D images have much complicated structure than their 2D counterparts, 3D IR is not just a simple generalization of the 2D IR problem. In this paper, we develop a 3D IR method that can handle cases with affine geometric transformations well. By its definition, an affine transformation maps a line to a line, and it includes rotation, translation and scaling as special cases. In practice, most geometric transformations involved in IR problems are affine transformations. Therefore, our proposed method can find many IR applications. It is shown that this method works well in various cases, including cases when the data size of a 3D image is reduced for different reasons. This latter property makes it attractive for many 3D IR applications, since 3D images are often big in data size and it is natural to reduce their size for fast computation.

Keywords Function approximation · Geometric transformation · Image mapping · Iterative algorithm · Kernel estimation · Least squares · Performance evaluation

1 Introduction

In many imaging applications, we need to compare two or more images of a same object so that useful information in the images can be combined and the difference among images can be detected. One such example is about the comparison of several MRI images [3, 4] of the head of a brain tumor patient that were taken at different times, so that the tumor growth can be monitored closely. Although those images are about the same object, pixels on one image may not geometrically match up with the corresponding ones on the others well, for reasons such as the relative move between the head and the imaging device at different imaging times. In order to compare two images properly for locating their difference accurately, the two images should be geometrically matched up first. Image registration (IR) is specifically for this purpose [29, 17]. It is an indispensable step for many imaging applications, including medical imaging [14], remote sensing [15], finger print or face recognition [16], image compression [10], video enhancement [13], and so forth.

In the literature, most IR methods are for analyzing 2D images [5, 6]. These methods can be roughly divided into two groups: feature-based and intensity-based methods. Feature-based methods first select two sets of features in the two images under consideration, and then find a geometrical transformation $\mathbf{T}$ to best match the two sets of features [1, 8, 21]. Commonly used features include landmarks or control points that can be selected manually or automatically by a computer [26], edge lines or curves that are often

Huajun Song
College of Information and Control Engineering, China University of Petroleum (East China)

Peihua Qiu
Department of Biostatistics, University of Florida

detected by gradient-based methods [12], regions, centroid or templates that are usually determined by ways of thresholding and segmentation [24], and degenerate pixels of the image intensity function [21]. Because feature extraction is often a time-consuming and challenging task with much arbitrariness involved, recent IR research focuses more on the search of the transformation $\mathbf{T}$ based directly on the observed image intensities of the two images. Such methods are often called intensity-based image registration (IBIR) methods. Commonly used IBIR methods include those based on parametric transformation families [9], and more flexible ones using nonparametric transformation families [2, 18, 22, 23, 25, 27].

In practice, most objects in our real life are 3D. We focused on 2D images in the past because only 2D images could be acquired at that time. Thanks to the rapid development of image acquisition techniques, 3D images have become more and more popular nowadays in certain applications (e.g., medical imaging). Consequently, 3D image registration is an important research problem with broad applications. However, 3D images have much more complicated structure than 2D images. For instance, edge locations are surfaces in 3D images which have more complicated structure than edge curves in 2D images. So far, there does not exist many 3D image registration methods in the literature yet. Some 2D image registration methods have been generalized to 3D cases and they were incorporated in the software package 3DSlicer (http://slicer.org/). A popular 3D IR method is based on the Iterative Closest Point (ICP) algorithm [7, 28]. This is a feature-based IR method based on the assumption that $\mathbf{T}$ has a parametric form. To use such a method, two sets of features need to be extracted first from the two related images. Then, the ICP algorithm alternates between estimating the parameters in $\mathbf{T}$ and searching for the optimal pointwise correspondence between the two sets of features. However, it is well-known that this method suffers from the following drawbacks: (i) the inconvenience in extracting the related features, (ii) the restriction in using a parametric geometric transformation, (iii) the heavy dependence on the quality of initialization in the algorithm, and (iv) the risk to obtain local minima instead of global minima.

In this paper, we propose a new 3D image registration method. This method is designed specifically for cases when the geometric transformation from one image to the other is an affine transformation, implying that any line on an image will still be a line after the transformation. We focus on affine transformations in this paper because they are the most common ones in practice. The affine transformation and our proposed method will be described in detail in Section 2. Some numerical results are presented in Section 3. Several remarks conclude the article in Section 4.

2 Proposed 3D Image Registration Method

2.1 The model

Mathematically, the 3D IR problem can be described as follows. Let $f_R(x,y,z)$ be a reference 3D image, and $f_M(x,y,z)$ be a moved 3D image. Then, the major goal of 3D IR is to find a geometrical transformation $\mathbf{T}(x,y,z) = (T_1(x,y,z), T_2(x,y,z), T_3(x,y,z))$ such that $f_M(\mathbf{T}(x,y,z))$ is as close to $f_R(x,y,z)$ as possible. There are two kinds of affine transformations: uniform and non-uniform. Uniform affine transformation is to enlarge or shrink image objects by a scale factor that is the same in all directions and at all locations. Most medical applications belong to this case. As a contrary, the scale factor in a non-uniform affine transformation depends on the location and/or direction. In this paper, we focus on uniform affine transformations, which include 3D rotation, translation and uniform scaling as special cases [11]. A uniform affine transformation has the following expression:

$$\begin{aligned}
T_1(x,y,z) &= s(x(\cos\alpha\cos\beta) + y(\sin\alpha\cos\beta) - z(\sin\beta)) + \Delta x,\\
T_2(x,y,z) &= s(x(\cos\alpha\sin\beta\sin\gamma - \sin\alpha\cos\gamma) + y(\sin\alpha\sin\beta\sin\gamma + \cos\alpha\cos\gamma) + z(\cos\beta\sin\gamma)) + \Delta y,\\
T_3(x,y,z) &= s(x(\cos\alpha\sin\beta\cos\gamma + \sin\alpha\sin\gamma) + y(\sin\alpha\sin\beta\cos\gamma - \cos\alpha\sin\gamma) + z(\cos\beta\cos\gamma)) + \Delta z,
\end{aligned} \tag{1}$$

where α, β, and γ are three rotation parameters, along the $x-$, $y-$, and $z-$axes, respectively, $\Delta x, \Delta y$, and Δz are three translation parameters along the three axes, and s is the scaling factor.

In practice, the true images $f_R(x,y,z)$ and $f_M(x,y,z)$ are usually not observed, and the observed images would have noise involved, as described by the following models:

$$\begin{aligned}
Z_M(x_i,y_j,z_k) &= f_M(x_i,y_j,z_k) + \varepsilon_M(x_i,y_j,z_k),\\
Z_R(x_i,y_j,z_k) &= f_R(x_i,y_j,z_k) + \varepsilon_R(x_i,y_j,z_k), \qquad \text{for i, j, k} = 1,2,\ldots,\text{n},
\end{aligned} \tag{2}$$

where $(x_i, y_j, z_k) \in \Omega$ are the $(i, j, k)-$th voxels, $Z_M(x_i, y_j, z_k)$ and $Z_R(x_i, y_j, z_k)$ are the observed reference and moved images, and $\varepsilon_M(x_i, y_j, z_k)$ and $\varepsilon_R(x_i, y_j, z_k)$ are random noise. Therefore, to solve the 3D IR problem, we need to estimate the 7 parameters $\alpha, \beta, \gamma, \Delta x, \Delta y, \Delta z$ and s in (1) from the observed images $Z_M(x_i, y_j, z_k)$ and $Z_R(x_i, y_j, z_k)$, so that $\{Z_M(\mathbf{T}(x_i, y_j, z_k))\}$ is as close to $\{Z_R(x_i, y_j, z_k)\}$ as possible.

2.2 Model estimation

First, let us write the transformation $\mathbf{T}(x, y, z) = (T_1(x, y, z), T_2(x, y, z), T_3(x, y, z))$ in the following form:

$$(T_1(x, y, z), T_2(x, y, z), T_3(x, y, z)) = (x, y, z) + (b(x, y, z), c(x, y, z), d(x, y, z)),$$

Then, $b(x, y, z) = T_1(x, y, z) - x, c(x, y, z) = T_2(x, y, z) - y, d(x, y, z) = T_3(x, y, z) - z$, and they denote the geometric moves along the $x-, y-$, and $z-$axes, respectively. It is obvious that estimation of $\mathbf{T}(x, y, z)$ is equivalent to estimation of $(b(x, y, z), c(x, y, z), d(x, y, z))$. In cases when $(b(x, y, z), c(x, y, z), d(x, y, z))$ are small and $f_M(x, y, z)$ has the first-order partial derivatives at (x, y, z), by the Taylor's expansion, we have

$$\begin{aligned} f_M(T_1(x, y, z), T_2(x, y, z), T_3(x, y, z)) = f_M(x, y, z) + f'_{Mx}(x, y, z)b(x, y, z) + \\ f'_{My}(x, y, z)c(x, y, z) + f'_{Mz}(x, y, z)d(x, y, z) + o(\parallel \mathbf{T}(x, y, z) - (x, y, z) \parallel), \end{aligned} \tag{3}$$

where $f'_{Mx}(x, y, z)$, $f'_{My}(x, y, z)$ and $f'_{Mz}(x, y, z)$ are the first-order partial derivatives of $f_M(x, y, z)$ with respect to x, y, and z, respectively, and $\| \cdot \|$ is the Euclidean norm. For the true transformation $\mathbf{T}(x, y, z)$ we have $f_R(x, y, z) = f_M(\mathbf{T}(x, y, z))$. By (3), $f_R(x, y, z)$ can be well approximated by $f_M(x, y, z) + f'_{Mx}(x, y, z)$ $b(x, y, z) + f'_{My}(x, y, z)$ $c(x, y, z) + f'_{Mz}(x, y, z)d(x, y, z)$ in such cases. Therefore, the 7 parameters in $(\hat{b}(x, y, z)$, $\widehat{c}(x, y, z)$, $\widehat{d}(x, y, z))$ can be chosen such that the approximation error

$$f_R(x, y, z) - [f_M(x, y, z) + f'_{Mx}(x, y, z)b(x, y, z) + f'_{My}(x, y, z)c(x, y, z) + f'_{Mz}(x, y, z)d(x, y, z)]$$

is as small as possible. In reality, however, $f_R(x, y, z)$, $f_M(x, y, z)$, $f'_{Mx}(x, y, z)$, $f'_{My}(x, y, z)$, $f'_{Mz}(x, y, z)$ are all unobservable. What observed are $Z_R(x_i, y_j, z_k)$ and $Z_M(x_i, y_j, z_k)$ in (2) that contain noise. To smooth out noise when estimating the parameters in $(b(x, y, z), c(x, y, z), d(x, y, z))$, we can use the least squares (LS) estimation as follows. For the time being, let us assume that $f'_{Mx}(x, y, z)$, $f'_{My}(x, y, z)$, $f'_{Mz}(x, y, z)$ have been estimated by $\widehat{f'_{Mx}}(x, y, z)$, $\widehat{f'_{My}}(x, y, z)$, $\widehat{f'_{Mz}}(x, y, z)$ beforehand. Then, $\Theta = (\alpha, \beta, \gamma, \Delta x, \Delta y, \Delta z, s - 1)$ can be estimated by the solution of

$$\begin{aligned} \min_{\Theta} \sum_{i,j,k=1}^{n} \Big[Z_M(x_i, y_j, z_k) - Z_R(x_i, y_j, z_k) - \widehat{f'_{Mx}}(x_i, y_j, z_k)b(x_i, y_j, z_k) - \\ \widehat{f'_{My}}(x_i, y_j, z_k)c(x_i, y_j, z_k) - \widehat{f'_{Mz}}(x_i, y_j, z_k)d(x_i, y_j, z_k) \Big]^2. \end{aligned} \tag{4}$$

In cases when all parameters α, β and γ are small, $\sin\alpha \approx \alpha$, $\sin\beta \approx \beta$, $\sin\gamma \approx \gamma$, $\cos\alpha \approx 1$, $\cos\beta \approx 1$, and $\cos\gamma \approx 1$. By these results, it can be checked that the LS estimator of Θ, which is the solution of (4), is

$$\widehat{\Theta} = (X^T X)^{-1} X^T Y, \tag{5}$$

where X is an $n^3 \times 7$ design matrix with the $[(i-1)n^2 + (j-1)n + k]$-th row being

$$\begin{aligned} &(-\widehat{f'_{Mx}}(x_i, y_j, z_k)y_j + \widehat{f'_{My}}(x_i, y_j, z_k)x_i, \widehat{f'_{Mx}}(x_i, y_j, z_k)z_k - \widehat{f'_{Mz}}(x_i, y_j, z_k)x_i, \\ &- \widehat{f'_{My}}(x_i, y_j, z_k)z_k + \widehat{f'_{Mz}}(x_i, y_j, z_k)y_j, \widehat{f'_{Mx}}(x_i, y_j, z_k), \widehat{f'_{My}}(x_i, y_j, z_k)x_i, \widehat{f'_{Mz}}(x_i, y_j, z_k), \\ &x_i\widehat{f'_{Mx}}(x_i, y_j, z_k) + y_j\widehat{f'_{My}}(x_i, y_j, z_k) + z_k\widehat{f'_{Mz}}(x_i, y_j, z_k)), \end{aligned}$$

and Y is an n^3 dimensional vector with the $[(i-1)n^2 + (j-1)n + k]$-th element being $Z_R(x_i, y_j, z_k) - Z_M(x_i, y_j, z_k)$.

To calculate the parameter estimators defined in (4) and (5), we still need to obtain estimators $\widehat{f'_{Mx}}(x,y,z)$, $\widehat{f'_{My}}(x,y,z)$, and $\widehat{f'_{Mz}}(x,y,z)$. To this end, we use the local linear kernel (LLK) estimation procedure in non-parametric regression analysis [19], and the LLK estimators are

$$\begin{aligned}
\widehat{f'_{Mx}} &= \frac{\sum_{i,j,k}(x_i-x)Z_M(x_i,y_j,z_k)\mathrm{K}_h(\frac{x_i-x}{h},\frac{y_j-y}{h},\frac{z_k-z}{h})}{\sum_{i,j,k}(x_i-x)^2\mathrm{K}_h(\frac{x_i-x}{h},\frac{y_j-y}{h},\frac{z_k-z}{h})},\\
\widehat{f'_{My}} &= \frac{\sum_{i,j,k}(y_j-y)Z_M(x_i,y_j,z_k)\mathrm{K}_h(\frac{x_i-x}{h},\frac{y_j-y}{h},\frac{z_k-z}{h})}{\sum_{i,j,k}(y_i-y)^2\mathrm{K}_h(\frac{x_i-x}{h},\frac{y_j-y}{h},\frac{z_k-z}{h})},\\
\widehat{f'_{Mz}} &= \frac{\sum_{i,j,k}(z_i-z)Z_M(x_i,y_j,z_k)\mathrm{K}_h(\frac{x_i-x}{h},\frac{y_j-y}{h},\frac{z_k-z}{h})}{\sum_{i,j,k}(z_k-z)^2\mathrm{K}_h(\frac{x_i-x}{h},\frac{y_j-y}{h},\frac{z_k-z}{h})},
\end{aligned} \tag{6}$$

where K is a kernel function with unit circular support, and $h>0$ is a bandwidth. As in the literature [19], we choose K to be $\mathrm{K}(x,y,z)=(1-x^2)(1-y^2)(1-z^2)$, which has some good theoretical properties.

2.3 Proposed 3D IR algorithm

The parameter estimators in (5) are derived based on the assumption that $\mathbf{T}(x,y,z)$ in (1) is small in the sense that all parameters in $\Theta=(\alpha,\beta,\gamma,\Delta x,\Delta y,\Delta z,s-1)$ are small. So, this algorithm is appropriate to use only in cases when that assumption is valid. For a general 3D IR problem in which the transformation may not be small, it is natural to consider an iterative version of that algorithm, based on the intuition that $\mathbf{T}(x,y,z)$ can be divided into many small transformations and each iteration of the algorithm can estimate one of these small transformations well. The iterative algorithm is described below.

Step 1. Compute estimators $\widehat{f'_{Mx}}(x,y,z)$, $\widehat{f'_{My}}(x,y,z)$, $\widehat{f'_{Mz}}(x,y,z)$ by (6).

Step 2. Obtain initial parameter estimators by (5). The corresponding estimator of $\mathbf{T}$ is denoted as $\widehat{\mathbf{T}}^{(0)}$.

Step 3. Define $Z_M^{(1)}(x_i,y_j,z_k)=Z_M(\widehat{\mathbf{T}}^{(0)}(x_i,y_j,z_k))$. In the next iteration, execute Steps 1 and 2 again, after $\{Z_M(x_i,y_j,z_k)\}$ are replaced by $\{Z_M^{(1)}(x_i,y_j,z_k)\}$. The resulting estimator of $\mathbf{T}$ is denoted as $\widehat{\mathbf{T}}^{(1)}$.

Step 4. In the vth iteration, the estimator of $\mathbf{T}$ is denoted as $\widehat{\mathbf{T}}^{(v)}$, and the parameter estimators are denoted as $\widehat{\Theta}^{(v)}=(\widehat{\alpha}^{(v)},\widehat{\beta}^{(v)},\widehat{\gamma}^{(v)},\widehat{\Delta x}^{(v)},\widehat{\Delta y}^{(v)},\widehat{\Delta z}^{(v)},\widehat{s}^{(v)}-1)$. The algorithm stops when $\max(\widehat{\alpha}^{(v)},\widehat{\beta}^{(v)},\widehat{\gamma}^{(v)})\le\varepsilon_1$, $\max(\widehat{\Delta x}^{(v)},\widehat{\Delta y}^{(v)},\widehat{\Delta z}^{(v)})\le\varepsilon_2$, and $|\widehat{s}^{(v)}|\le\varepsilon_3$, where $\varepsilon_1,\varepsilon_2,\varepsilon_3>0$ are three small numbers.

From the above iterative algorithm and the estimation procedure (4)-(5), we can see that in each iteration, the algorithm tries to adjust the moved image geometrically so that the image intensities of the adjusted moved image are closer to those of the reference image, in terms of the sum of squares of their differences. So, the sequence of the sums of squares would not increase over iterations. This property together with the stopping rule used in the algorithm would guarantee the convergence of the algorithm, which was confirmed in our numerical studies.

Also, we want to point out that our method is appropriate to use when all parameters in Θ are relatively small because of the nature of the Taylor's expansion that it is based on (cf., expression (3)). In most applications, the relative move between the imaging device and the imaging objects, or the scaling factor, is small. So, our method should be relevant.

3 Numerical Study

In this section, we present some numerical results about the proposed 3D IR method described in the previous section. To this end, we use three popular measures [20], including the root residual mean squares (RRMS), the correlation coefficient (CC), and the entropy of image difference (EID). RRMS is defined to be

$$RRMS=\{\frac{1}{n^3}\sum_{i,j,k=1}^{n}[Z_R(x_i,y_j,z_k)-Z_M(\widehat{\mathbf{T}}(x_i,y_j,z_k))]^2\}^{1/2}.$$

Table 1: Proportion p (in percentage) of the original voxels in the reference image, and the numbers of selected rows in the $x-, y-$, and $z-$axes in the brain image example.

	number of rows		
p	$x-$axis	$y-$axis	$z-$axis
0.0097	12	12	10
0.0172	16	16	10
0.0269	20	20	10
0.0526	28	28	10
0.0687	32	32	10
0.0870	36	36	10
0.0969	38	38	10
0.1289	40	40	12
0.1560	44	44	12

Basically, RRMS is the Euclidean distance between $\{Z_R(x_i, y_j, z_k)\}$ and $\{Z_M(\widehat{\mathbf{T}}(x_i, y_j, z_k)\}$. Therefore, if its value is smaller, then the image registration is regarded better. The CC measure is defined to be the Pearson's sample correlation coefficient of the bivariate data $\{Z_R(x_i, y_j, z_k), Z_M(\widehat{\mathbf{T}}(x_i, y_j, z_k))\}$. Intuitively, if the estimator $\widehat{\mathbf{T}}(x_i, y_j, z_k)$ is good, then $Z_M(\widehat{\mathbf{T}}(x_i, y_j, z_k)$ would be close to $Z_R(x_i, y_j, z_k)$. Consequently, CC would be close to its maximum value 1. The EID measure become popular recently. It is defined as

$$EID = -\sum_{d\in D} p(d)\log\, p(d),$$

where $D = \{Z_R(x_i, y_j, z_k) - Z_M(\widehat{\mathbf{T}}(x_i, y_j, z_k), i, j, k = 1, 2, \ldots, n\}$, and $p(d)$ is the relative frequency of d in D. So, EID is basically the negative entropy of D. Intuitively, if $\widehat{\mathbf{T}}(x, y, z)$ is a good estimator of $\mathbf{T}(x, y, z)$, then the randomness in the elements of D should be large. Consequently, EID should be small because the entropy $\sum_{d\in D} p(d)\log\, p(d)$ is a good measure of the randomness of D. Therefore, by this measure, the image registration is better if the EID value is smaller.

In the first example, the 3D reference image is downloaded from http://www.slicer.org/slicerWiki/images/4/43/MR-head.nrrd. It is a 3D MRI image of the head of a patient, and has $256 \times 256 \times 130$ voxels. The 20th, 30th, ..., and 110th slices along the z-axis are shown in the first row of Figure 1. To evaluate the performance of the proposed IR method, we first create a moved image by geometrically shifting, rotating and scaling the reference image along the $x-, y-$, and $z-$axes, respectively, with its front-top-left corner as the center for rotation and scaling. The reference image is rotated along the x, y, and $z-$axes by 2 degrees each, shifted along the three axes by 3, 4 and 5 voxels, respectively, and the scaling factor is set to be 0.95. When defining the moved image, the nearest-neighbor interpolation procedure is used. The 10 corresponding slices of the moved image are shown in the second row of Figure 1. By comparing the images in the first 2 rows of Figure 1, it can be seen that they look quite different.

In this example, besides the proposed IR method, we also consider the scaling rigid-body 3D IR method in the software package 3DSlicer. The version of the software package that is used here is its newest release 4.5 that is available at http://www.slicer.org/. To make the comparison of the two methods fair, we choose the option of the nearest-neighbor interpolation in 3DSlicer as well, as in the proposed IR method. To study the performance of the two methods when the data size is reduced, we apply each method to a small proportion p of the two original images. When selecting the sub-samples from the original voxels, the selection in the reference image is always the same as that in the moved image, and the selected indices of the voxels are always equally spaced in the $x-, y-, z-$axes, respectively, starting from the first row in each axis. The specific selections of the sub-samples are described in Table 1.

For each sub-sample described in Table 1, we apply the two methods, and the results in terms of RRMS, CC and EID are shown in Figure 2. From the plots in the figure, it can be seen that 1) both methods perform better when p is larger, 2) the method in 3DSlicer performs slightly better when $p \geq 0.0526\%$, but its performance deteriorates very fast when $p \leq 0.0526\%$, and 3) our proposed IR method is quite stable even when p is as small as 0.0172%. This example shows that our proposed method can be considered to use in big-data applications when data size is large or when the image registration needs to be fast (e.g., in cases to online monitor sequences of images).

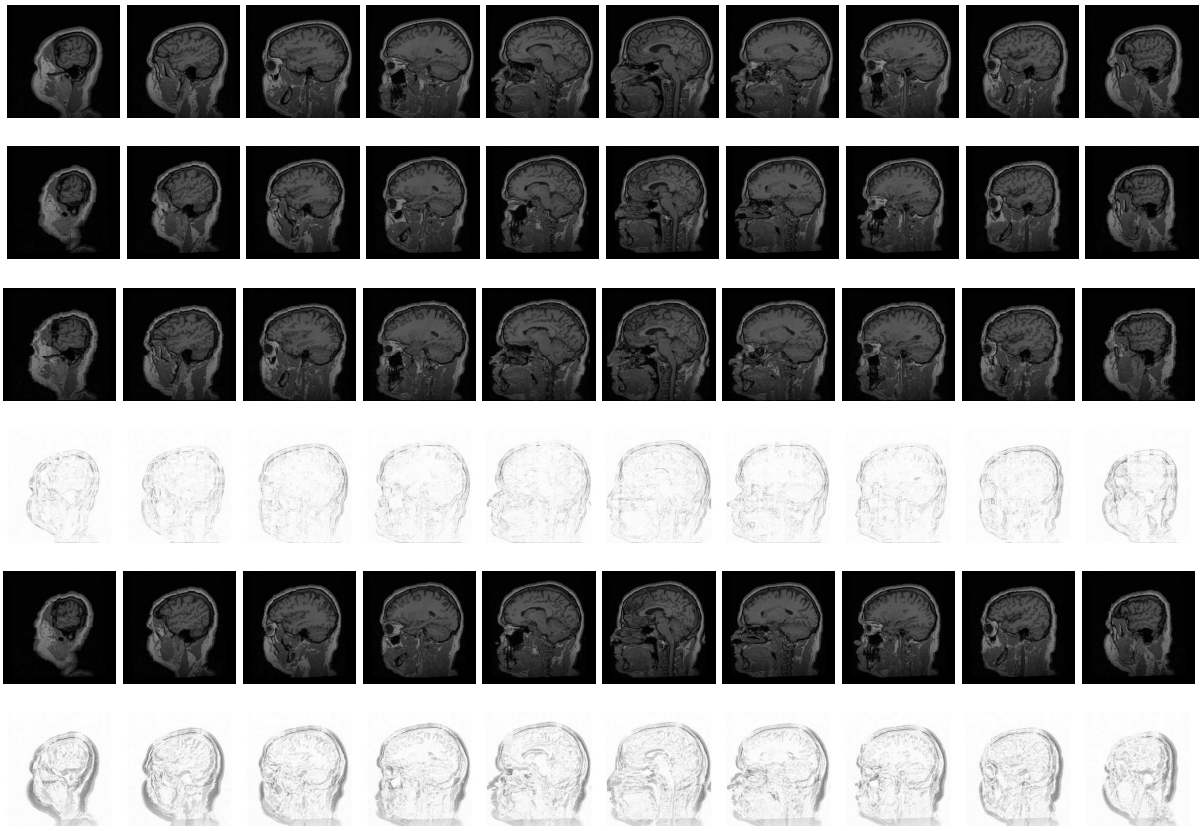

Fig. 1: Head MRI image example. The first row shows 10 slices of the reference image, the second row shows the 10 corresponding slices of the moved image, the third and fifth rows are the corresponding slices of the restored reference images by the proposed method and the scaling rigid-body method in 3DSlicer when $p = 0.0172\%$. The fourth and sixth rows are the corresponding slices of the residual images of the two methods. The 10 slices in each row denote the 20th, 30th, ..., and 110th slices of the related 3D image along the $z-$axis.

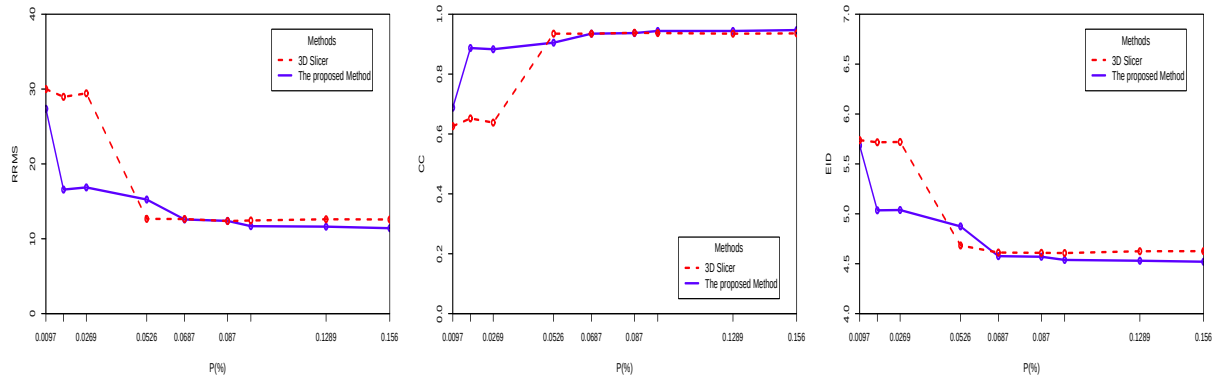

Fig. 2: RRMS, CC and EID values of the proposed IR method and the scaling rigid-body IR method in the software package 3DSlicer.

In the case when $p = 0.0172\%$, the 10 slices of the restored reference image $Z_M(\widehat{\mathbf{T}}(x, y, z))$ and the corresponding slices of the difference image $Z_R(\mathbf{T}(x, y, z)) - Z_M(\widehat{\mathbf{T}}(x, y, z))$ by the proposed method are shown in the third and fourth rows of Figure 1. The corresponding results by the scaling rigid-body IR method in 3DSlicer are shown in the fifth and sixth rows of the same figure. It can be seen that the proposed

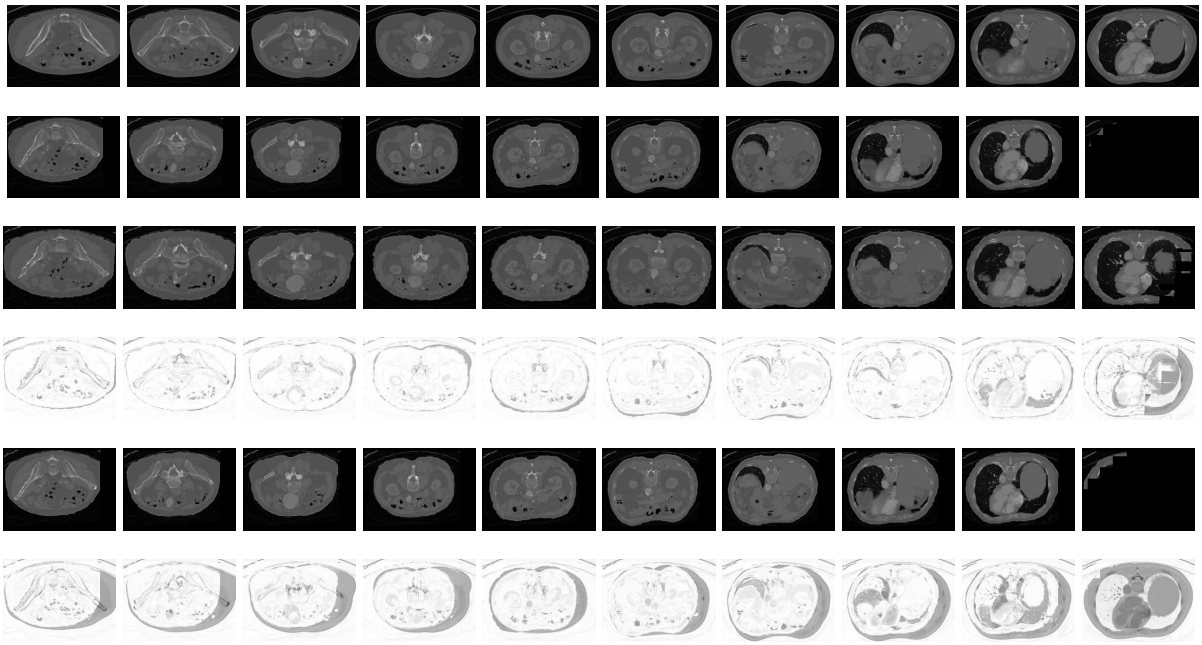

Fig. 3: Abdomen MRI image example. The first row shows 10 slices of the reference image, the second row shows the 10 corresponding slices of the moved image, the third and fifth rows are the corresponding slices of the restored reference images by the proposed method and the scaling rigid-body method in 3DSlicer when $p = 0.1026\%$. The fourth and sixth rows are the corresponding slices of the residual images of the two methods. The 10 slices in each row denote the 10th, 20th, ..., and 100th slices of the related 3D image along the $z-$axis.

method has a better performance, compared to the method in 3DSlicer, since its restored reference image looks closer to the true reference image and its difference image has weaker non-random pattern. This result is consistent with those shown in Figure 2.

By the way, all numerical examples presented in this section were computed using a computer with an Intel CPU i5-2450 and with 4G of memory. Compared to the methods in 3DSlicer, our proposed method is fast to compute. For instance, when the sampling proportion $p = 0.0687\%$ in the above example, the proposed method takes about 3 seconds to finish the image registration task, while the method in 3DSlicer takes about 4 seconds. When the sampling proportion is $p = 0.0172\%$, the proposed method takes 0.9 seconds while the method in 3DSlicer takes about 2.5 seconds.

Next, we consider another example about an abdomen MRI image of a patient. The 3D reference image, which is an abdomen MRI image of a patient, is downloaded from
http://slicer.kitware.com/midas3/download/, and it has $220 \times 160 \times 107$ voxels. Its 10th, 20th, ..., 100th slices along the $z-$axis are shown in the first row of Figure 3. To create a moved image, we first rotate it along the $x-$, $y-$, and $z-$axes by 3, 2, and -2.5 degrees, respectively. As in the previous example, the rotation and scaling center is set at the front-top-left corner. Then, the rotated image is shifted along the three axes by -4, 3 and 2 voxels, respectively, and finally the resulting image is shrinked with a scaling factor of 0.93. Its 10th, 20th, ..., 100th slices along the $z-$axis are shown in the second row of Figure 3.

We then apply the proposed method and the scaling rigid-body IR method in 3DSlicer to this example. Similar to the previous example, the two original images are reduced in size by sub-sampling and the sub-sampling ratio is p (in percent). The selection of the sub-samples is made in a similar way to that in the previous example, with the numbers of rows in the three axes listed in Table 2. Some results of the two methods corresponding to those in Figures 1 and 2 are shown in Figures 3 and 4. It can be seen that our proposed method performs much better in this example as well.

Table 2: Proportion p (in percentage) of the original voxels in the reference image, and the numbers of selected rows in the $x-$, $y-$, and $z-$axes in the abdomen image example.

	number of rows		
p	$x-$axis	$y-$axis	$z-$axis
0.0335	16	16	10
0.0523	20	20	10
0.1026	28	28	10
0.1177	30	30	10
0.2374	36	36	14
0.2713	36	36	16
0.3400	38	38	18

Table 3: RRMS, CC and EID values of the proposed IR method and the scaling rigid-body IR method in the software package 3DSlicer in five random cases.

	α	β	γ	Δx	Δy	Δz	s	3DSlicer			IR		
								RRMS	CC	EID	RRMS	CC	EID
1	-0.03	-1.29	2.64	-2	2	-1	0.95	36.03	0.70	6.40	26.01	0.81	5.32
2	-0.58	-0.45	1.02	2	-3	-2	0.99	16.70	0.96	4.86	13.61	0.94	3.77
3	-1.33	-2.34	-0.66	1	-1	0	0.94	39.51	0.65	6.52	19.37	0.89	4.66
4	-2.51	-0.46	-0.81	-1	-2	0	0.99	21.40	0.91	5.41	16.18	0.92	4.68
5	1.48	-1.97	-1.92	-1	-1	-2	0.98	12.46	0.97	4.64	24.50	0.81	4.76

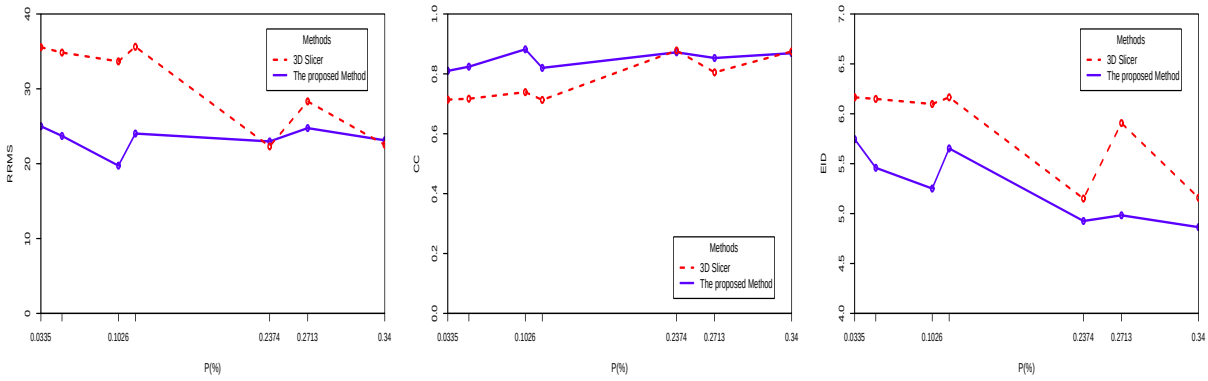

Fig. 4: RRMS, CC and EID values of the proposed IR method and the scaling rigid-body IR method in the software package 3DSlicer.

To study the robustness of our proposed method to different rigid-body transformations, we randomly generated 5 sets of values of the transformation parameters as follows: each of (α, β, γ) was generated from the Uniform distribution on $[-3, 3]$, each of $(\Delta x, \Delta y, \Delta z)$ was generated from the Uniform distribution on $\{-3, -2, -1, 0, 1, 2, 3\}$, and the scale factor s was generated from the Uniform distribution on $[0.9, 1]$. The performance measures of the scaling rigid-body IR method in 3DSlicer and our proposed method are presented in Table 3. From the table, it can be seen that our proposed method outperforms the 3DSlicer method in 4 out of 5 cases. The averaged values of RRMS, CC and EID over all 5 cases are 19.93, 0.87 and 4.76, respectively, for our proposed method, and they are 25.22, 0.84 and 5.57 for the 3DSlicer method. So, we can see that our proposed method has a better overall performance.

4 Concluding Remarks

In the previous sections, we have described our proposed IR method for analyzing 3D images. This method is appropriate for handling cases with uniform affine transformations involved, which are the most common cases

in practice. It is shown that our proposed method is reliable to use in applications where data compression is necessary. This property makes it attractive for applications with big data, such as online monitoring of a sequence of 3D MRI images. In some other applications, a non-uniform affine transformation might be necessary for properly describing the geometric transformation involved in the IR problem. In such cases, it is still unknown to us how to generalize the proposed method properly, which is left for our future research.

References

1. Althof, R., Wind, M., Dobbins, J.: A rapid and automatic image registration algorithm with subpixel accuracy. IEEE Transactions on Medical Imaging **19**, 308–316 (1997). DOI 10.1109/42.585765
2. Avants, B., Epstein, C., Grossman, M., Gee, J.: Symmetric diffeomorphic image registration with cross-correlation: evaluating automated labeling of elderly and neurodegenerative brain. Medical Image Analysis **12**, 26–41 (2008). DOI 10.1016/j.media.2007.06.004
3. Behroozi, M., Daliri, M., Boyaci, H.: Statistical analysis methods for the fmri data. Basic & Clinical Neuroscience **4**, 67–74 (2011)
4. Behroozi, M., Mohammad, R.: Software tools for the analysis of functional magnetic resonance imaging. Basic and Clinical Neuroscience **3**, 71–83 (2012)
5. Behroozi, M., Mohammad, R.: Predicting brain states associated with object categories from fmri data. Journal of integrative neuroscience **13**, 645–667 (2014)
6. Behroozi, M., Mohammad, R.: Rdlpfc area of the brain encodes sentence polarity: a study using fmri. Brain imaging and behavior **9**, 178–189 (2015)
7. Besl, P., McKay, N.: A method for registration of 3-d shapes. T-PAMI **14**, 239–256 (1992). DOI 10.1109/34.121791
8. Davis, M., Khotanzad, A., Flamig, D., Harms, S.: Physics-based coordinate transformation for 3-d image matching. IEEE Transactions on Medical Imaging **16**, 317–328. (1997). DOI 10.1109/42.585766
9. Denton, E., Sonoda, L., Rueckert, D., Rankin, S., Hayes, C., Leach, M., Hill, D., Hawkes, D.: Comparison and evaluation of rigid, affine, and nonrigid registration of breast mr images. Journal of Computer Assisted Tomography **23**, 800–805 (1999). DOI 10.1109/TIE.2012.2185019
10. Dufaux, F., Konrad, J.: Efficient, robust, and fast global motion estimation for video coding. IEEE Transactions on Image Processing **9**, 497–501 (2000). DOI 10.1109/83.826785
11. Eggert, D., Lorusso, A., Fisher, R.: Estimating 3-d rigid body transformations: a comparison of four major algorithms. Machine Vision and Applications **9**, 272–290 (1997). DOI 10.1007/s001380050048
12. Hsieh, J., Liao, H., Fan, K., Ko, M., Hung, Y.: Image registration using a new edge-based approach. Computer Vision and Image Understanding **67**, 112–130 (1997). DOI 10.1006/cviu.1996.0517
13. Irani, M., Peleg, S.: Motion analysis for image enhancement: resolution, occlusion and transparency. Journal of Visual Communication and Image Representation **4**, 324–335 (1993). DOI 10.1006/jvci.1993.1030
14. Klein, A., Andersson, J., Ardekani, B., et al.: Evaluation of 14 nonlinear deformation algorithms applied to human brain mri registration. NeuroImage **46**, 786–802 (2009). DOI 10.1016/j.neuroimage.2008.12.037
15. Li, H., Manjunath, B., Mitra, S.: A contour-based approach to multisensor image registration. IEEE Transactions on Image Processing **4**, 320–334 (1995). DOI 10.1109/83.366480
16. Liu, L., T.Jiang, Yang, J., Zhu, C.: Fingerprint registration by maximization of mutual information. IEEE Transactions on Image Processing **15**, 1100–1110 (2006). DOI 10.1109/TIP.2005.864161
17. Modersitzki, J.: Fair: Flexible algorithms for image registration. SIAM: Philadelphia. (2009). DOI 10.1137/1.9780898718843
18. Pan, W., Qin, K., Chen, Y.: An adaptable-multilayer fractional fourier transform approach for image registration. IEEE Transactions on Pattern Analysis and Machine Intelligence **31**, 400–412 (2009). DOI 10.1109/TPAMI.2008.83
19. Qiu, P.: Image processing and jump regression analysis. New York: John Wiley and Sons. (2005)
20. Qiu, P., Nguyen, T.: On image registration in magnetic resonance imaging. IEEE Proceedings of 2008 International Conference on BioMedical Engineering and Informatics **2**, 753–757 (2008). DOI 10.1109/BMEI.2008.33
21. Qiu, P., Xing, C.: Feature based image registration using non-degenerate pixels. Signal Processing **93**, 706–720 (2013a). DOI 10.1016/j.sigpro.2012.09.013
22. Qiu, P., Xing, C.: On nonparametric image registration. Technometrics **55**, 174–188 (2013b). DOI 10.1080/00401706.2012.727768

23. Rajwade, A., Banerjee, A., Rangarajan, A.: Probability density estimation using isocontours and isosurfaces: application to information-theoretic image registration. IEEE Transactions on Pattern Analysis and Machine Intelligence **31**, 475–491 (2009). DOI 10.1109/TPAMI.2008.97
24. Saeed, N.: Magnetic resonance image segmentation using pattern recognition, and applied to image registration and quantitation. NMR in Biomedicine **11**, 157–167 (1998). DOI 10.1002/(SICI)1099-1492(199806/08)11:4/53.0.CO;2-L
25. Tustison, N., Avants, B., Gee, J.: Directly manipulated free-form deformation image registration. IEEE Transactions on Image Processing **18**, 624–635 (2009). DOI 10.1109/TIP.2008.2010072
26. Wu, G., Qi, F., Shen, D.: Learning-based deformable registration of mr brain images. IEEE Transactions on Image Processing **25**, 1145–1157 (2006). DOI 10.1109/TMI.2006.879320
27. Xing, C., Qiu, P.: Intensity based image registration by nonparametric local smoothing. IEEE Transactions on Pattern Analysis and Machine Intelligence **33**, 2081–2092 (2011). DOI 10.1109/TPAMI.2011.26
28. Yang, J., Li, H., Jia, Y.: Go-icp:solving 3d registration efficiently and globally optimally. International Conference on Computer Vision (ICCV) pp. 1457–1464 (2013). DOI 10.1109/ICCV.2013.184
29. Zitova, B., Flusser, J.: Image registration methods: a survey. Image and Vision Computing **21**, 977–1000 (2011). DOI 10.1016/S0262-8856(03)00137-9